Supporting Information

Plasmon Rulers as a Probe for Real-Time Microsecond Conformational Dynamics of Single Molecules

Emiel W.A. Visser[1,2*], Matěj Horáček[1,2], Peter Zijlstra[1,2*]

1. Dept. of Applied Physics, Eindhoven University of Technology
2. Institute for Complex Molecular Systems (ICMS), Eindhoven University of Technology

**Corresponding authors:*
e.w.a.visser@tue.nl
p.zijlstra@tue.nl

Supporting Method 1: Monte Carlo simulations

The distribution of possible system geometries was simulated using a Monte Carlo simulation method, implemented in Matlab (in-house developed code available upon request). Potential system states were generated according to the system geometry. The geometry of the system was defined in terms of objects (rod, sphere, and surface) and tethers that link the system together (with appropriate properties). The particles were simulated as spheres and the rods as cylinders capped with half spheres of the appropriate size. The surface was defined at the $z = 0$ plane.

The tether molecules were simulated as a Kratky-Porod chain of connected straight elements of length l_s with a persistence length of P. The straight elements were connected in series and the joints between segments bend with an associated bending energy:

$$E_{\text{bend}} = \frac{k_b T P}{2 l_s} \theta^2, \tag{1}$$

where k_b is the Boltzmann constant, T the temperature, and θ the bend angle of the joint between two consecutive elements. The chain was constructed segment by segment and the orientation of the next segment in the chain was drawn from a Boltzmann distribution:

$$P \propto e^{-E_{\text{bend}}/k_b T}. \tag{2}$$

Individual segments were added to the chain until the required chain length was reached. For the simulation of PEG tethers in the system $l_s = 0.1$ nm, $P = 0.1$ nm, for ssDNA $l_s = 0.63$ nm and $P = 3$ nm were used.

After the construction of a potential system state, the state was checked against the boundary conditions. The boundary conditions excluded the overlap between chain elements, rod, particles, and the surface. If any violation of the boundary conditions was found, the state was discarded, and another state was generated. If the state was found to be correct the parameter of interest, *i.e.* the position of the particle, was extracted. This process continued until typically $2 \cdot 10^5$ to $1 \cdot 10^6$ valid states were found.

Using the Monte Carlo simulation method, we approximated the position distribution of a nanoparticle that is tethered to a surface immobilized particle. From the position distribution, we extracted the effective interaction potential as it is experienced by the particle tethered to the rod.

Supporting Method 2: Determination of the effective interaction potential

The effective interaction potential was calculated from the position distribution of the tethered particle. The effective potential $E(x, y, z)$ can be immediately calculated from the position distribution by inverting the Boltzmann distribution:

$$E(x, y, z) = -k_b T \ln P(x, y, z) + C. \tag{3}$$

in which C is akin to a constant of integration and can be freely chosen.

The Monte Carlo simulations (see Supporting Method 2) approximated the position distribution through stochastic sampling of the distribution. Typically, $2 \cdot 10^5$ to $1 \cdot 10^6$ positions were sampled. First the position distribution data was organized in a 3-dimensional histogram of the position data, with a spatial resolution of either 0.5 or 0.25 nm. To diminish the effect of the stochastic sampling,

smoothing was applied. Histogram smoothing was based on a smoothing implementation for fixed grid data, using the discrete cosine transform from Garcia *et al*.[1] Smoothing was performed using geometry-appropriate weighting of the data points; histogram bins in which zero states were found, and of which the center of the bin falls within the volume excluded by the rod are given a weight of zero in the smoothing. The probability density was then smoothed, without introducing artefacts that arise from the sudden drop to zero at the edge of the excluded volumes. In the smoothed position distribution, all bins of which at least 5 vertices fell within the rod (approximately more than half the bin) were set to zero. The accuracy of the smoothed result was validated by comparing the difference between the original and smoothed position distribution and ensuring that no systematic deviations were observed.

The potential was then calculated from the smoothed position distribution using the relationship of Supporting Equation 3 in which C was chosen to set the lowest potential at zero. This resulted in a good approximation of the real potential and was used as the effective potential in the Brownian Dynamics simulations. The bins of the histogram are referred to as 'voxels' from here on to clarify the 3D volume enclosed.

Supporting Method 3: Brownian Dynamics simulation

Next, Brownian Dynamics simulations were used to simulate the motion of the particle as it experiences the restrictive effect of the tether. Our implementation of the Brownian Dynamics is a forward Euler implementation of the Brownian motion of the particle that experiences the effective potential determined from the Monte Carlo simulations. The simulation incremented the position of the particle by a time-step Δt based independently on (1) the Brownian displacement, (2) the displacement due to the effective force

$$\vec{F} = -\nabla E \tag{4}$$

acting on the particle. The Brownian displacement $\vec{r}$ was determined using the mean squared displacement equation

$$\langle \vec{r}^2 \rangle = 6D\Delta t, \tag{5}$$

by randomly choosing the displacement $\Delta\vec{r}_{\mathrm{Brownian}}$ from a three-dimensional normal distribution with a $6D\Delta t$ standard deviation, where D is the diffusion constant of the particle in the system. The displacement due to the external force was determined using

$$\Delta\vec{r}_{\mathrm{Force}} = \vec{F}/\zeta\,, \tag{7}$$

where ζ is the drag coefficient

$$\zeta = 6\pi\eta r, \tag{8}$$

with η the viscosity and r the radius of the particle. The drag coefficient is related to the diffusion constant as

$$D = k_{\mathrm{b}}T/\zeta\,. \tag{9}$$

The total displacement during each timestep Δt was thus

$$\Delta\vec{r} = \Delta\vec{r}_{\mathrm{Force}} + \Delta\vec{r}_{\mathrm{Brownian}} \tag{10}$$

As the effective potential (and thus force) was defined in a square voxel grid we linearly interpolated the force acting on the particle to the exact position of the particle.

The timestep was optimized to minimize computational time and optimize the accuracy of the result. The aforementioned forward Euler method assumes that $\vec{F}$ is constant, which is not the case. The timestep needs to be small enough to minimize the error due to a force that changes in time. Therefore, the timestep was chosen using:

$$\Delta t(\vec{x}) = k \cdot \frac{2\zeta}{\left|\nabla\left|\vec{F}(\vec{x})\right|\right|}, \tag{11}$$

where k is an estimation of the maximum relative error made during a timestep, and the timestep is determined at a position $\vec{x}$. The time-step was determined for all positions and was stored in a reference table for quick-access during the simulations. To ensure an adequate time-resolution for the interpretation of the data a maximum time step of 0.1 ns was used.

The rod and the substrate form a hard boundary for the gold particle which translates to a sudden increase to an infinite potential E. To avoid problems with infinite gradients in the calculation, the walls were implemented and handled separately. A map of wall-voxels with infinite potential was determined before the simulation. If during any particle move the particle moves into a wall-voxel, the move is not executed and time is not incremented. This method approximates the repulsive Pauli exclusion interaction between the primary and the tether particle. This ignore-move implementation somewhat under-samples movements close to and towards the wall. We estimate the error using the expected Brownian motion; at a maximum timestep of 0.1 ns we expect a mean-squared average Brownian displacement of 0.12 nm for a particle with a diameter of 5 nm, which provides an upper limit on the error in the diffusive move near the wall. We regard this as sufficiently small as it is below the van der Waals radius of an individual gold atom (166 pm) and below the voxel size (250 or 500 pm).

The result of the Brownian Dynamics simulation is the simulated position of the particle as a function of time. The particle position was stored after every 10 ns in simulated motion to reduce the amount of generated data.

Supporting Method 4: BEM simulations

The plasmonic response of the system was numerically determined using the Boundary Element Method (BEM). BEM appears to be a natural choice for metallic nanoparticles with sizes ranging from a few to a few hundreds of nanometers, and for frequencies in the optical and near-infrared regime.[2,3] In BEM the materials are characterized by their dielectric functions, and the desired geometry is reduced to its surface which is discretized into a series of polygons. Maxwell's equations are then solved at the particle boundaries.

As the BEM implementation we used the MNPBEM toolbox designed for the Matlab™ programming environment.[3] The primary particle, either rod or sphere, was placed on a glass substrate in water, and the tethered particle was placed at the position of interest. The effect of the ssDNA tether on the optical response of the particle is negligible and was therefore not modelled. For gold we used the dielectric function measured by Johnson and Christy,[4] the glass substrate is characterized by the dielectric function of BK7 glass,[5] the surrounding water is considered to be non-dispersive and is characterized by a dielectric constant $\varepsilon_m = 1.77$. Since the presence of PEG coating on the particles

only shifts the dimer's plasmon wavelength and leaves the relative results unaffected, the PEG anti-fouling layer was not taken into account. Illumination was performed by a plane wave with a polarization parallel to the long-axis of the dimer.

We evaluated the full spectra of individual dimers (Figure S1a) to find the optimal probe wavelength positioned on the red wing of the dimer's plasmon. Next the (normalized) scattered light intensity was determined for different 3D positions of the tethered particle (Figure S1b-c). The possible positions of the tether particle around the primary particle were sampled to represent the map of the possible positions in the Brownian Dynamics simulations. For a separation between the primary particle and the tethered sphere below 4 nm the possible tethered particle positions were discretely sampled on a 1 nm grid, between 4 and 8 nm with a 2 nm grid, and the rest of the position space with a 4 nm discretization. The scattering and absorption cross sections were calculated at the probe wavelength for all positions of the tethered particle in the grid and were subsequently normalized to their respective references. These calculations were performed for all considered dimer geometries yielding a look-up table of the optical response as function of the position of the tethered particle.

DOI: 10.1021/acs.nanolett.8b03860

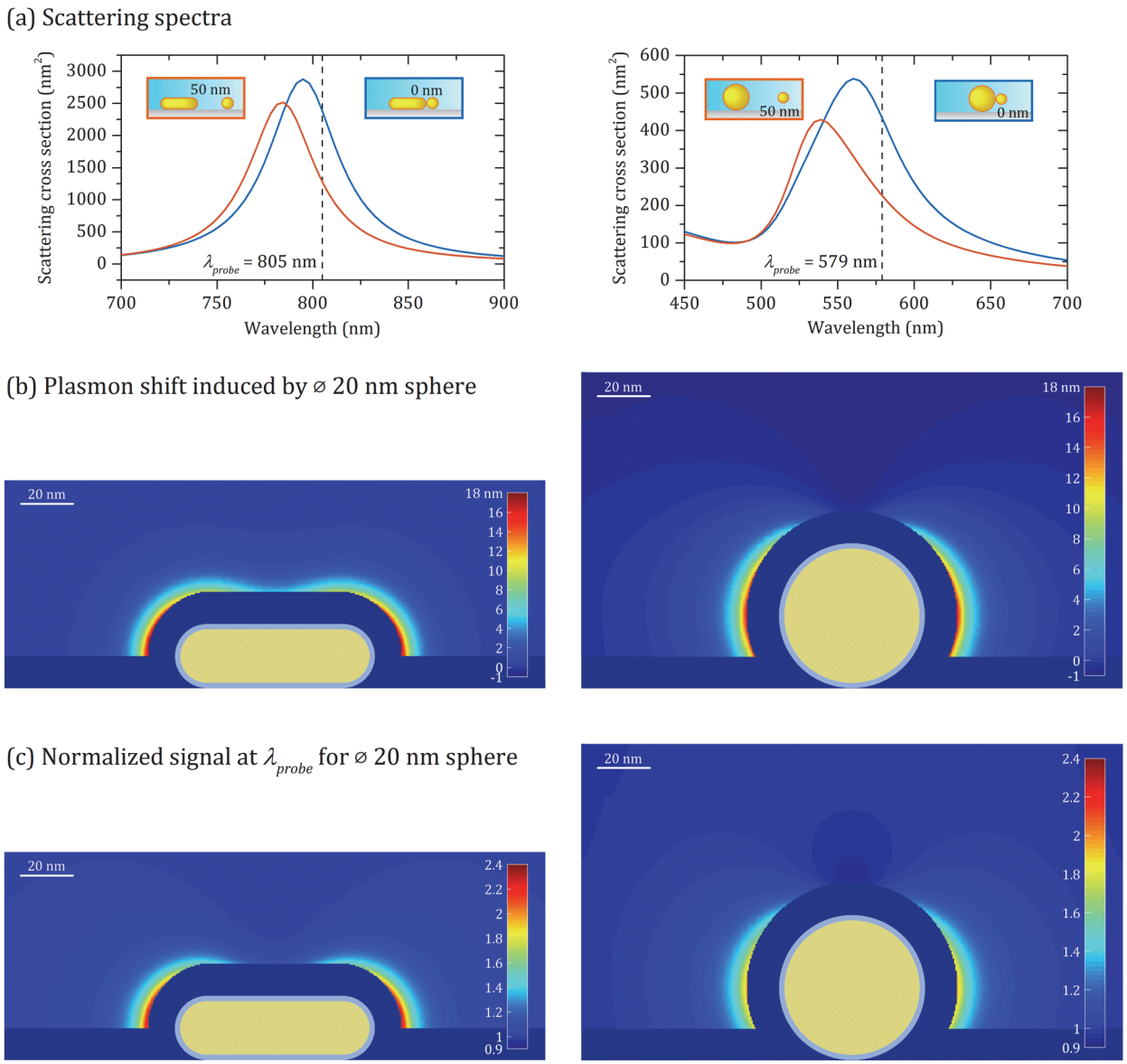

Figure S1: Numerical BEM calculations for both plasmonic sensors for a ⌀ 20 nm tethered sphere. (a) Scattering cross section in the proximal and the distal state of the tethered particle from a primary particle surface. Dashed lines represent optimum probe wavelengths. Spatial distributions of (b) plasmon shifts and (c) normalized intensity change at the probe wavelength induced by the tethered sphere (points in maps correspond to the geometrical center of the tethered sphere). The areas that the sphere cannot reach due to volume exclusion are visible as dark areas around the particles. Note that 2D projections are shown, whereas the calculations employ 3D distributions.

Supporting Note 5: Detected intensity modulations induced by conformational changes

Finally, the detected intensity as a function of time was determined by combining the Brownian Dynamics simulations with the position dependent scattered intensity determined using the BEM simulations. For every position of the tether particle the BEM results were interpolated to determine the scattering cross-section at that position. Interpolation of the BEM data was performed using the Matlab™ 'scatteredInterpolant' function using the natural interpolation method. The result is the scattering cross-section as a function of time: $\sigma_{\mathrm{scat}}(t, \lambda_{\mathrm{probe}})$.

The measured optical signal in terms of the number of detected photons is calculated as

$$N_{\mathrm{det}}(t) = t_{\mathrm{int}} \cdot \overline{\sigma_{\mathrm{scat}}}\left(t, \lambda_{\mathrm{probe}}\right) \cdot n_{\mathrm{illum}} \cdot \eta_{\mathrm{det}}. \tag{12}$$

The scattering cross-section at the probe wavelength $\sigma_{\mathrm{scat}}\left(t, \lambda_{\mathrm{probe}}\right)$ was averaged over the integration time t_{int}. The photon flux $n_{\mathrm{illum}} = 3.0 \cdot 10^{26} - 7.7 \cdot 10^{27}\ \mathrm{m^{-2}\ s^{-1}}$ describes the incident intensity (see Supporting Note 6). We have chosen a detection efficiency of $\eta_{det} = 0.01$ as a conservative estimate which encompasses the collection efficiency of the objective, optical transmission losses and detector efficiency.

Shot-noise was added to the detected signal by randomly drawing from a normal distribution with zero-mean and a variance of $\sqrt{N_{\mathrm{det}}}$, congruent with experimental shot noise. The result is the experimentally recorded signal including all relevant noise sources.

Supporting Note 6: Incident intensity and relation to particle heating

The incident intensity determines at large N_{det}, but is limited by the maximum acceptable heating of the particle dimer it induces. We have set a limit on the maximum allowed heating of $\Delta T = 2$ K. To estimate the particle temperature, we approximate the geometry of the rod/sphere-dimer as a single sphere with equivalent volume. The maximum allowed illumination intensity I_{illum} ($\mathrm{W \cdot m^{-2}}$) that limits heating to 2 K is then given by:[6]

$$I_{\mathrm{illum}} = \frac{4\pi k R \Delta T}{\sigma_{\mathrm{abs}}}, \tag{13}$$

with $k = 0.56\ \mathrm{W \cdot m^{-1} \cdot K^{-1}}$ the thermal conductivity of water, R the radius of the equivolume sphere, and σ_{abs} the absorption cross-section of the dimer ($\mathrm{m^2}$, calculated using BEM simulations) at λ_{probe}. The illumination intensity can be expressed in the number of photons $\mathrm{m^{-2}}$:

$$n_{\mathrm{illum}} = \frac{I_{\mathrm{illum}}}{hc/\lambda}. \tag{15}$$

At this maximum incident intensity, the scattered intensity of the dimer is:

$$I_{\mathrm{scat}} = \frac{4\pi k R \Delta T}{\sigma_{\mathrm{abs}}} \sigma_{\mathrm{scat}}\left(t, \lambda_{\mathrm{probe}}\right), \tag{14}$$

with σ_{scat} the scattering cross-section of the dimer ($\mathrm{m^2}$). Dividing by the photon energy $E = hc/\lambda$, with h Planck's constant and c the speed of light, we calculate the number of scattered photons per second.

Supporting Table 1

Table S1 summarizes the characteristic system parameters for the rod-sphere dimer system.

Table S1: Overview of the parameters used in the calculations for the rod-sphere dimer system. The scattering and absorption cross-sections are determined for the reference system which includes only the rod.

Rod L x Ø (nm)	Sphere Ø	λ_{probe}	σ_{scat} ($\cdot 10^3$nm²)	σ_{abs} $\left(\cdot 10^3\ \mathrm{nm}^2\right)$	N_{scat} $\left(s^{-1}\right)$
70 x 20	5 nm	805 nm	1.23	15.6	$8.0 \cdot 10^{10}$
70 x 20	10 nm	805 nm	1.23	15.6	$8.0 \cdot 10^{10}$
70 x 20	14 nm	805 nm	1.23	15.6	$8.0 \cdot 10^{10}$
70 x 20	18 nm	805 nm	1.23	15.6	$8.0 \cdot 10^{10}$
70 x 20	20 nm	805 nm	1.23	15.6	$8.0 \cdot 10^{10}$

Supporting Table 2

Table S2 summarizes the characteristic system parameters for the sphere-sphere dimer system.

Table S2: Overview of the parameters used in the simulations of the sphere-sphere dimer system. The scattering and absorption cross-sections are determined for the reference system which includes only the rod.

Ø Sphere 1	Ø Sphere 2	λ_{probe}	σ_{scat} ($\cdot 10^3$nm²)	σ_{abs} $\left(\cdot 10^3\ \mathrm{nm}^2\right)$	N_{scat} $\left(s^{-1}\right)$
50 nm	10 nm	579 nm	0.205	1.86	$1.4 \cdot 10^{11}$
50 nm	20 nm	579 nm	0.227	1.99	$1.5 \cdot 10^{11}$
50 nm	30 nm	582 nm	0.275	2.12	$1.8 \cdot 10^{11}$
50 nm	40 nm	582.5 nm	0.423	2.84	$2.3 \cdot 10^{11}$
50 nm	50 nm	588 nm	0.701	3.67	$3.1 \cdot 10^{11}$
50 nm	60 nm	592.5 nm	1.31	5.39	$4.5 \cdot 10^{11}$

Supporting Note 7: Correlation time

The correlation time of the detected intensity was determined by calculating the autocorrelation function and fitting the correlogram with a single exponential function $R(t) = e^{-\tau/t}$. A typical correlogram and fit is shown in figure S2.

DOI: 10.1021/acs.nanolett.8b03860

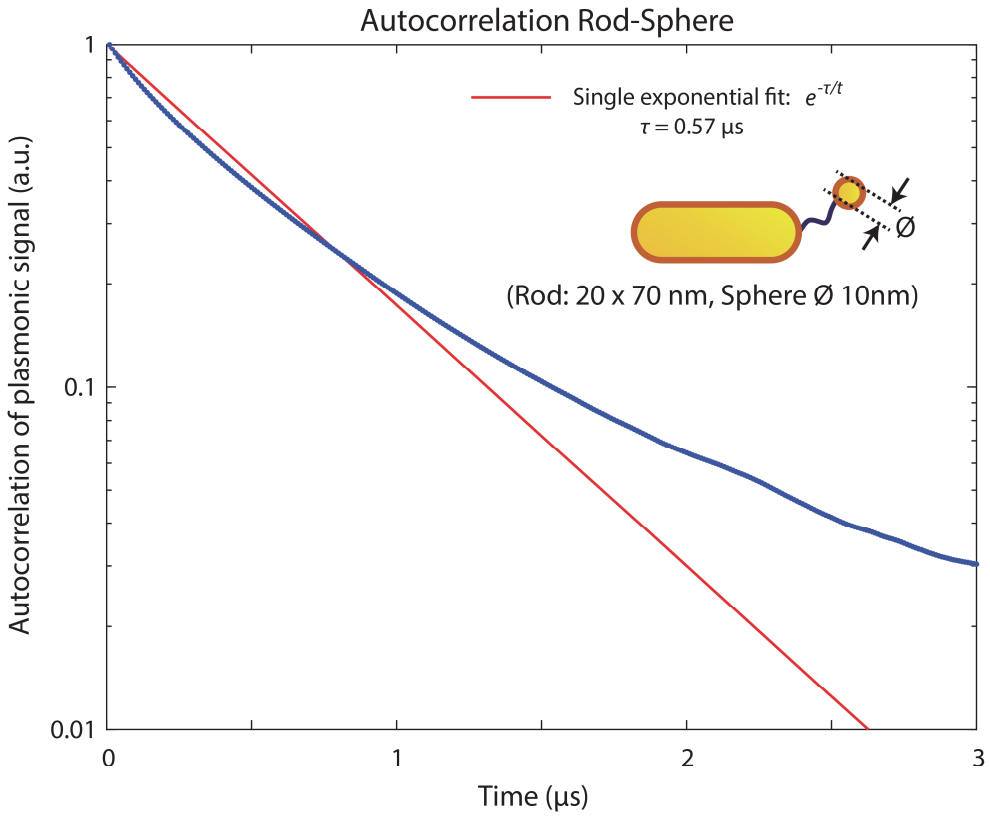

Figure S2: Correlogram of the autocorrelation of the plasmonic signal for a rod-sphere nanoruler. The correlation time is determined from the single-exponential fit at $\tau = 0.57$ µs. Note that the autocorrelation function is not strictly mono-exponential due to the complex tether potential and near-field profile of the dimers. The half-time provides an alternative, model-independent, parameter to characterize the decay time but leads to nearly identical results and does not affect our conclusions.

Supporting Note 8: SNR of the sphere-sphere nanoruler

We simulated the rod-sphere system to the sphere-dimer in which a primary particle of diameter 50 nm is bound to the substrate and a tether-particle (diameter 10 – 60 nm) is bound via the state switching tether (open state 50 nt ssDNA, closed state 7 nt ssDNA). A diameter of 50 nm for the gold particle dimer yields a scattering cross-section that is close to the 20 x 70 nm^2 rod when both are excited on the red wing of their plasmon resonance. A direct comparison of the SNR curves and τ_p for the different geometries is shown in figure S2. We find that the sphere-sphere geometry yields a SNR curve that is comparable to the nanorod-sphere system for a dimer with a 20 nm tether-particle. The signal's correlation time $\tau_p = 0.9$ µs for this dimer owing to the similarly sized tether particle, indicating that accessible time resolution is comparable to the rod-sphere geometry.

DOI: 10.1021/acs.nanolett.8b03860

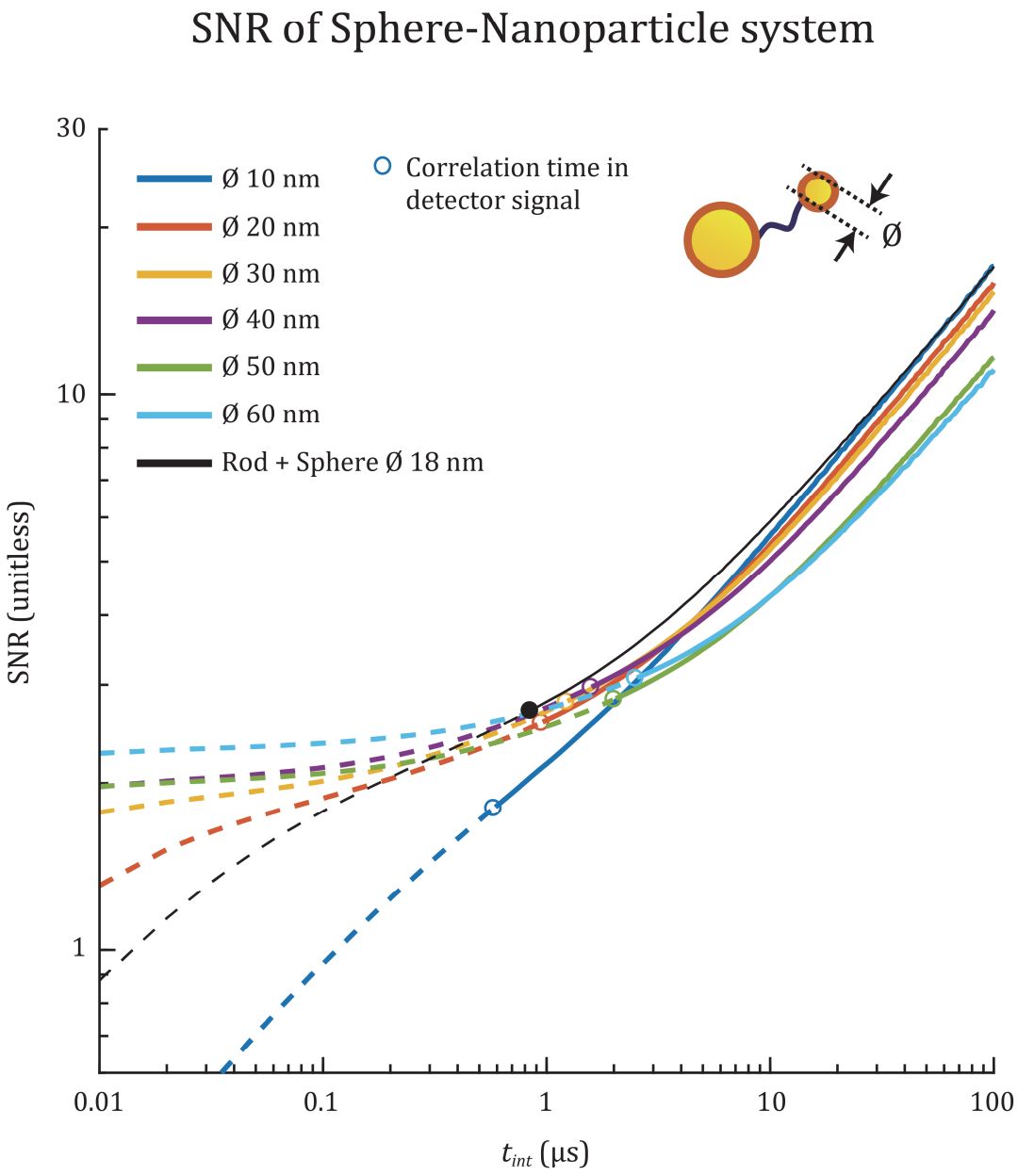

Figure S3: The SNR of the detection of a state change between the open and closed state as a function of the integration time for particle diameters of 10, 20, 30, 40, 50 and 60 nm and the SNR for the Rod-Nanoparticle system with the 18 nm tether particle. The transition to the diffusion-limited regime (dashed lines) is indicated by the correlation time in the detector signal τ_p (open circles), which indicates the time needed by the tether particle to explore the available space in the open state.

Supporting References

(1) Garcia, D. Robust Smoothing of Gridded Data in One and Higher Dimensions with Missing Values. *Comput. Stat. Data Anal.* **2010**, *54* (4), 1167–1178.

(2) García de Abajo, F. J.; Howie, A. Retarded Field Calculation of Electron Energy Loss in

Inhomogeneous Dielectrics. *Phys. Rev. B* **2002**, *65* (11), 115418.

(3) Hohenester, U.; Trügler, A. MNPBEM – A Matlab Toolbox for the Simulation of Plasmonic Nanoparticles. *Comput. Phys. Commun.* **2012**, *183* (2), 370–381.

(4) Johnson, P. B.; Christy, R. W. Optical Constants of the Noble Metals. *Phys. Rev. B* **1972**, *6* (12), 4370–4379.

(5) Schott. Optical Glass: Data Sheets https://www.schott.com/d/advanced_optics/ac85c64c-60a0-4113-a9df-23ee1be20428/1.3/schott-optical-glass-collection-datasheets-english-17012017.pdf (accessed May 20, 2015).

(6) Bejan, A. *Heat Transfer*; John Wiley & Sons, Inc: New York, 1993.